Assessment of Fatigue Life of Railway Drawbar Support According to UIC and TSI Requirements.

Vladislav Maznichki

***Abstract*—The study presents the development of computational models for the support component of the drawbar device used in railway wagons. The aim is to create reliable finite element method (FEM) models that replicate the real operational behavior of the support plate under static and dynamic loads. The methodology includes an analysis of relevant European and international standards (EN 15566, UIC 520, UIC 826, TSI), identification of load cases for drawbar systems with nominal forces of 1.0, 1.2 and 1.5 MN, and evaluation of material fatigue using Miner's rule and the Goodman criterion. Numerical simulations were carried out in ANSYS Workbench™ and DesignLife™, and material properties of ductile cast iron GJS 600-3 were applied. The obtained results indicate that the developed models realistically describe the stress-strain state of the support element and predict reliable fatigue performance for the required 30-year service life.**

***Keywords*— Computation model, FEM, Fatigue, Drawbar, Railway wagons.**

I. INTRODUCTION

The draw gear and buffing devices constitute essential components of railway rolling stock. They are widely applied both in the traction units of locomotives and in passenger and freight wagons. In recent years, increasing efforts have been directed towards the automation of wagon coupling by means of automatic couplers. Several patents have been issued in this field [1], and in-depth investigations aimed at their design and dimensioning have been reported in the literature [2], [3]. Despite the tendency to implement automatic couplers in newly manufactured wagons, the predominant solution across Europe remains the standardized draw gear (**DG**), equipped with a screw coupling.

Given the significant loads they are subjected to, DGs are required to comply with stringent design and testing standards. To ensure interoperability among manufacturers, these devices are standardized, obliging each producer to adhere to prescribed connection dimensions and clearance limitations. The principal parameters of DGs are specified in detail in the International Union of Railways (UIC) leaflets [4], [5] the European Directive [6], and the Technical Specifications for Interoperability (TSI) [7], which collectively define the essential requirements for their individual elements. Directive [6] distinguishes three DG categories according to load capacity: 1 MN, 1.2 MN, and 1.5 MN. Nonetheless, the system includes components that fail under tensile loads of approximately 1 MN. One such component is the suspension, highlighted in blue in Fig. 1. A comprehensive investigation of this element was conducted in [8], where crack growth was analyzed based on actual load data recorded from train operation via a locomotive monitoring device. In addition, tensile strength tests were performed in [8], [9] in accordance with the recommendations of [6].

Although the remaining elements are generally over-dimensioned in comparison to the suspension, fractures have nonetheless been observed in every component of the assembled unit. Evidence of this can be found in studies investigating the failure of draw hooks [10] [11] Furthermore, [12] presents a systematic failure analysis of DGs.

A DG typically consists of several principal groups: the screw coupling, the draw hook, draw bar, the DG support, and the energy absorber, each serving a specific function. These elements are illustrated in Fig. 1.

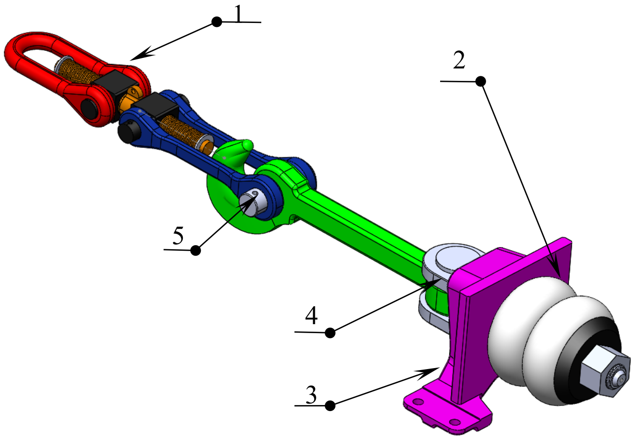

Fig. 1. Standardized draw gear: 1 – screw coupling, 2 – polymer energy absorber, 3 – DG support, 4 – draw bar, 5 – draw hook.

The present study focuses on the DG support (component no. 3 in Fig. 1. The standards [4], [6] describe two variants of this part, both manufactured as welded assemblies; however, neither satisfies the contemporary requirement of transmitting a force of 1.5 MN, as stipulated in [4], [5] [6], [7]. To address this deficiency, design modifications are required in order to enhance the strength characteristics of the support while preserving the critical dimensions necessary for interoperability. Verification calculations are therefore indispensable.

II. ANALYSIS OF REGULATORY DOCUMENTS

In order to ensure proper design sizing and the appropriate selection of load cases, a detailed analysis of [6] has been carried out, where procedures for conducting physical tests are also specified. The support of the draw

Received: 01.07.2026
Published: 26.07.2026
https://doi.org/10.47978/TUS.2026.76.03.010

Vladislav Maznichki is with the Technical University of Sofia, CoE "National center of mechatronics and clean technologies, Sofia, 1000, 8 Kl. Ohridski Blvd, Bulgaria (v.maznichki@tu-sofia.bg)

gear is tested in the same manner as the Draw bar and the draw hook, with a design service life of 30 years, unless other requirements are stipulated for DGs intended to transmit forces of up to 1.5 kN. Table I presents the force values that each component must satisfy.

This approach provides the basis for assessing the component within the plastic deformation range, emphasizing that permanent deformation itself is not considered structural failure.

TABLE I
CLASSIFICATION AND DESIGNATION OF COUPLING SYSTEM [6]

Coupling system designation	Min. breaking load of screw coupling [kN]	Max. breaking load of screw coupling [kN]	Min. breaking load in traction of the draw gear and draw hook [kN]
1000kN	850	990	1000
1200kN	1020	1190	1200
1500kN	1350	1490	1500

In order to demonstrate the probability of fatigue in the component, the testing procedures established for the drawbar and the draw hook are applied, as the support is evaluated under the same load cases. The test is conducted in accordance with Fig. 2, which illustrates the application of forces on the component.

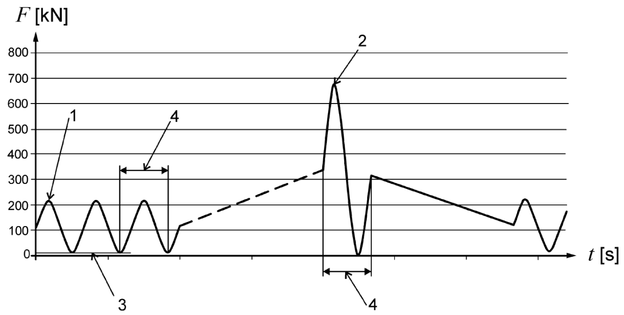

Fig. 2. Force–time diagram for fatigue evaluation. 1 – maximum value of load case 1; 2 – maximum value of load case 2; 3 – lower force limit determined by the pre-tension force; 4 – cycle frequency not exceeding 4 Hz; [6]

As illustrated in Fig. 2, the different load cases alternate during the dynamic test performed to verify the probability of fatigue occurrence. The number of cycles and the force magnitudes are summarized in Table II.

TABLE II
CONDITION OF DYNAMIC TEST FOR ALL PARTS EXCEPT SCREW COUPLING [6]

Lifecycle in years	RANGE OF FORCES TO BE APPLIED		
	1000kN	ΔF1 = 200kN	ΔF2 = 675kN
	1200kN	ΔF1 = 240kN	ΔF2 = 810kN
	1500kN	ΔF1 = 300kN	ΔF2 = 1015kN
		N_1 in cycles	***N_2 in cycles***
20	all	10^6	$1{,}45 \times 10^3$
30	all	$1{,}5 \times 10^6$	$2{,}15 \times 10^3$

In the present study, the component under consideration is designed for the most unfavorable loading conditions. From the review conducted, it can be concluded that the most critical conditions correspond to a load of 1.5 MN and a service life of 30 years. For the purposes of the investigation, the following load cases must be considered, as summarized in Table III.

TABLE III
LOAD CASES FOR SUPPORT PLATE FOR LOAD OF 1,5MN

Load case	Force magnitude	Evaluation criteria
1	1500kN	Minimum braking force of 1500kN
2	1125kN	Accumulation damage <1
3	1015kN	Accumulation damage <1
4	300kN	Accumulation damage <1

It should be noted that the accumulated fatigue from all load cases must be evaluated using an appropriate assessment method in order to determine the serviceability of the component.

III. METHODOLOGY FOR PRODUCT ASSESSMENT

The assessment methodology is based on that presented in [13], further extended to enable the consideration of accumulated fatigue as described in [14]. Since the evaluation is performed within the plastic deformation range, the probability of fatigue occurrence is assessed using Miner's rule. This method allows prediction of accumulated fatigue in the component for each individual load case, based on the calculated stress levels. Comparable assessments have been reported in the literature, where accumulated fatigue was determined [15] and S–N curves for various materials were established [15], [16]. This approach provides a realistic estimate of whether the component can reliably operate within the specified service interval of 30 years, as summarized in Table II. The fatigue evaluation of the material is carried out in accordance with Equation 1.

$$D = \frac{n_1}{N_1} + \frac{n_2}{N_2} + \cdots + \frac{n_k}{N_k} = \sum_{i=1}^{k} \frac{n_i}{N_i} \leq 0 \qquad (1)$$

where:

D – accumulated fatigue in the considered node;

n_i – applied number of cycles for investigated load cases.

N_i – endurance number of cycles according to S-N.

The methodology proposed in [13] and [14] is comprehensive and encompasses procedures for investigating fatigue initiation in welded joints. However, it does not explicitly account for plastic deformation, which is relevant to the present study. In order to be applicable here, the methodology requires certain modifications. The adapted methodology can be summarized in the following steps.:

1. Identification of the load cases.
2. Analysis of the wagon's design documentation in order to determine the load-distribution elements.
3. The structural elements are divided into "n" groups based on the material properties.
4. Determination of the material properties for all applied materials, according to European or national standards: Rp, Rm, stress–strain diagram (if not available, constructed using the three-parameter method in [17]), and S–N curves for fatigue assessment.
5. The investigated joints are categorized into *m* groups according to their structural characteristics, specifically the type of weld applied and the level of stress concentration associated with it.
6. A simulation model for stress–strain analysis is

developed. In the modeling process, the weld zones and stress concentrators must be explicitly represented, which ensures a complete and objective evaluation of the structural strength according to the permissible stress criterion.

7. Execution of verification calculations. If the calculated values exceed the yield limit, the plastic deformation of the material must be taken into account.
8. Refinement of the simulation model by introducing time-dependent loading and unloading curves, consistent with the cyclic patterns defined in Fig. 2.
9. Theoretical determination of the principal stresses $(\sigma_1, \sigma_2, \sigma_3)_{ij}$ for each node.
10. Sorting into databases according to type (base material and weld)
11. Sorting into databases according to material properties.
12. For each investigated weld, the maximum principal stress (σ_{max}). is identified. All normal stresses from the stress tensor (σ_x, σ_y, σ_z) are then projected in the direction of (σ_{max}). The minimum value from these projections is taken as the minimum stress for the cycle (σ_{min}).
13. Determination of an evenly distributed number of cycles for the various load cases from Table III. The maximum number of cycles must correspond to the full-scale testing procedure of the investigated component.
14. Determination of the maximum number of cycles for each load case from the fatigue curves according to Eurocode 3 Part 1-9 [18], or alternatively by using the S–N diagram of the applied material.
15. Calculation of accumulated fatigue using Equation (1).

In the Eurocode provisions cited within the selected methodology, fatigue is considered only for steel structures. Based on Table I and the chosen approach of evaluating the component within the plastic deformation range, attention must also be given to the material characteristics. To achieve a reliable assessment, the most unfavorable material conditions should be assumed, since the failure limits are typically provided as ranges; therefore, the lower bound is to be applied unless tensile tests and S–N fatigue diagrams have been experimentally obtained, as presented in numerous studies [19], [20], [21] where the material properties are explicitly determined.

The material selected for the component is cast iron GJS 600-3. Some of the key properties used in the computational model (IM) are as follows: yield strength Rp0.2 = 395 MPa; ultimate tensile strength Rm = 650 MPa [22], which correspond to the values presented in [23]. Plastic deformation is accounted for through a bilinear material model. The S–N curve for the selected material is shown in Fig. 3.

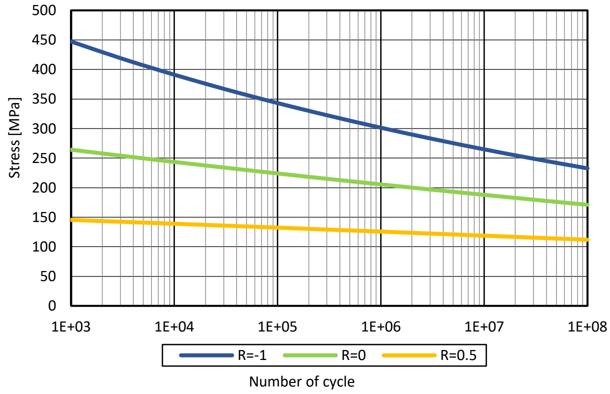

Fig. 1. S-N curve, iron GJS 600-3 [22]

IV. Developing Computational Models

In the process of developing computational models, it is essential to conduct a detailed analysis of the design documentation and to identify the force-transmitting elements. This allows for the proper definition of boundary conditions and ensures that the computational model closely reflects the actual behavior of the investigated component in service.

For the building of the computational model, ANSYS® Workbench™ was used, while the geometry was generated using ANSYS® SpaceClaim®. The general view of the model geometry is presented in Fig. 4.

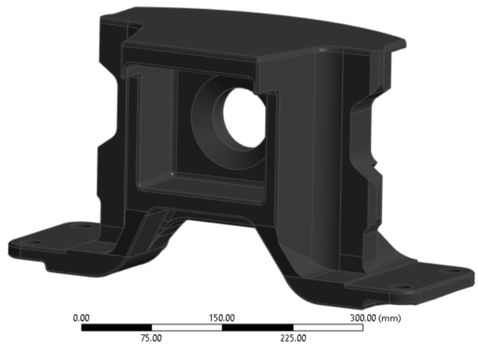

Fig. 4. Draw gear Support.

A computational model is composed of several key elements: the geometry, external and internal loads, boundary conditions, and the discretization of the model.

When the draw gear support is modeled as an isolated component and boundary conditions from the wagon stoppers are applied directly to it, significant errors may arise. Such simplification can cause unrealistic local stiffening, which prevents the correct bending behavior of the component and consequently leads to inaccurate stress results.

To ensure that the model reflects the actual behavior, a portion of the wagon's cantilever structure must be reproduced. Regardless of the wagon type, its design complies with interoperability requirements, meaning that the force transmission remains nearly identical. This approach enables the definition of contact interactions between the individual elements, including friction, as well as the introduction of additional loads from the pre-tension of the bolts that fasten the support to the wagon frame. The computational model of the draw gear support is shown in Fig. 5.

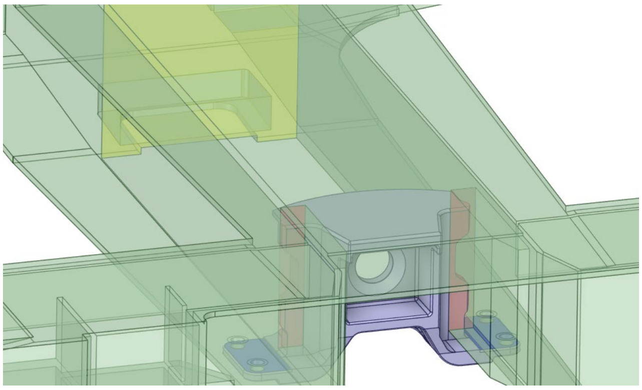

Fig. 5. Computational model of the draw gear support.

The boundary conditions in the computational model must reproduce the real service loading conditions as accurately as possible. To this end, constraints in all three translational directions were applied at the ends of the two UPN profiles forming the housing of the draw gear support (colored in yellow). This representation ensures that the global stiffness of the wagon structure is reflected in the model while avoiding unrealistic simplifications.

In the contact zone between the support and the end section of the wagon, a no-penetration condition was imposed (colored in dark blue and purple). Friction was also introduced to replicate the effect of bolt pre-tension. The bolts themselves were modeled as beam elements with circular cross-sections corresponding to the actual bolt diameter. The pre-tension was simulated by applying two opposite forces along the axis of each bolt element, converging toward its mid-point. The ends of the beam elements were connected to contact areas on the cantilever structure and the draw gear support, thereby replicating the washer and bolt head contact surfaces. In this way, the preload effect was transferred realistically, pressing the two components together and improving the accuracy of the stress distribution.

The primary load from the draw gear was applied as a force of 1.5 MN, in accordance with Table I. To simulate all relevant operating scenarios, the load magnitude was varied to reproduce the load cases presented in Table III. In order to account for plastic deformation, the load application was divided into two steps: loading and unloading. This approach allows for the capture of potential nonlinear material behavior and provides a more realistic fatigue assessment.

The discretized computational model is presented in Fig. 6. The mesh was generated using tetrahedral elements, and a mesh convergence study was conducted to ensure the accuracy and stability of the solution. Particular attention was given to refining the mesh in the stress concentration regions, as these areas are critical for the assessment of fatigue performance.

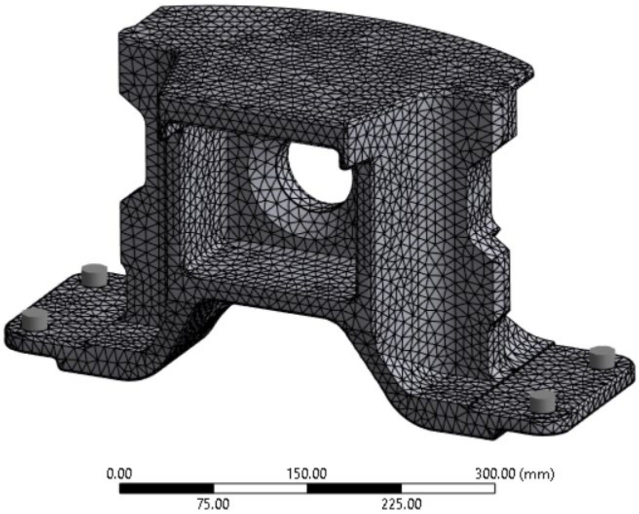

Fig. 2. Discretized geometry of the computation model.

The finite element mesh was generated with a total of 94,921 elements and 166,920 nodes. The maximum element size was set to 10 mm, while the minimum element size was refined to 2 mm in order to capture local stress concentrations with sufficient accuracy.

V. Results of the Computational Model

During the analysis, all load cases specified in Table III were executed. When the applied force exceeded 1.05 MN, plastic deformation was observed, as illustrated in Fig. 7.

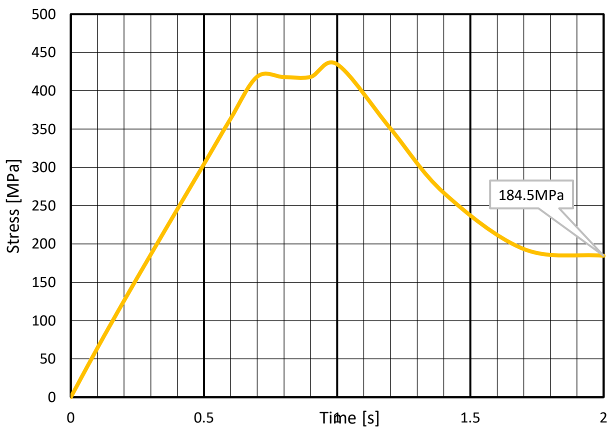

Fig. 7. Graph of plastic deformation under load case LC 1.

In Fig. 7 is presented a maximum stress in entire computational model for all steps of LC1 as a function of time. Residual stresses are clearly visible after unloading (t=2s, step of unloading process), which provides direct evidence of plastic deformation in the investigated component. The presence of such residual stresses confirms that the material has undergone irreversible changes in its stress–strain state, exceeding the elastic limit. This behavior is critical for the fatigue assessment, as residual stresses significantly influence crack initiation and propagation under cyclic loading. The distribution of von Mises stresses for Load Case 1 is presented in Fig. 8, illustrating the regions of maximum stress concentration and providing the basis for further evaluation of fatigue performance.

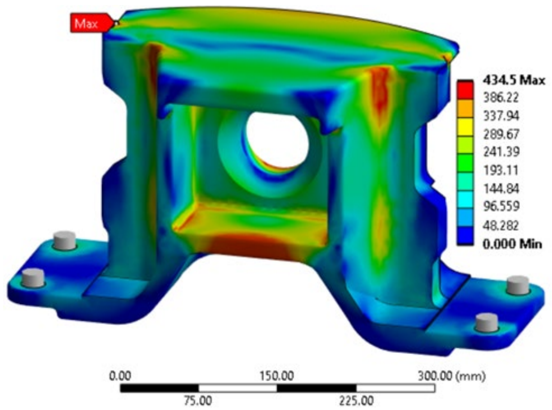

Fig. 8. (Von Mises) Stress distribution at t = 1 s under load case LC 1

In order to evaluate the probability of fatigue occurrence, the accumulated damage was estimated through Miner's rule, while the Goodman criterion was applied to account for mean stress effects. This requires the comprehensive analysis of results from all load cases defined in Table III. To perform the fatigue evaluation, ANSYS nCode DesignLife™ was employed, enabling the simulation of fatigue damage accumulation under multiaxial and variable amplitude loading conditions.

TABLE IV
LOAD CASES FOR SUPPORT PLATE FOR LOAD OF 1,5MN

Load case	Max stress t = 1s	Max stress t = 2s	Accumulated damage/cicle	LIfe
1	434,50MPa	136,37MPa	≈0,0090/2150	239370
2	417.65MPa	11.69MPa	≈0.0032/2150	682590
3	409,74MPa	-	≈0.0020/2150	1114900
4	123,06MPa	-	-	>10000000

The analysis of the results shows that under load case LC 4, where the applied force has a magnitude of 0.3 MN, the stress level does not exceed the fatigue limit, despite the large number of cycles specified in Table II. For load case LC 3, the number of cycles is 2150, which leads to an accumulated fatigue damage of approximately 0.0020—well below the critical threshold defined by condition (1).

For the purposes of comparison, in evaluating the accumulated fatigue under load cases LC 1 and LC 2, the results were normalized to the same number of cycles as defined for LC 3 (2150 cycles), even though these values are not considered in the actual fatigue life assessment. This approach enables a direct comparison of fatigue behavior across different load cases.

Fig. 9 presents the accumulated fatigue for 2150 cycles under load case LC 1.

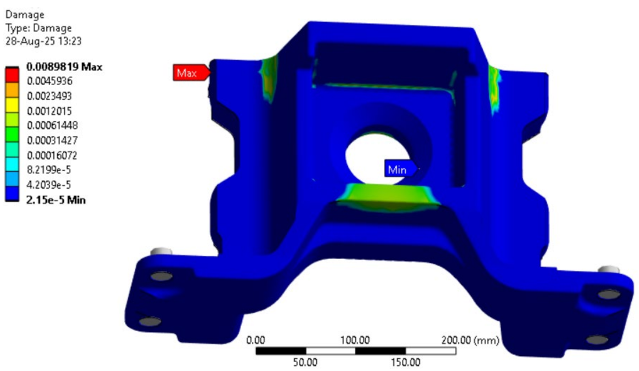

Fig. 9. Accumulated fatigue under load case LC 1.

In the entirely investigated component, the accumulated damage for the most significant load cases, considering both the number of cycles and the force magnitude, indicates that the model is predominantly colored in dark blue, meaning that approximately 96% of the material is below the endurance limit.

In the remaining 4% of the component, some accumulated fatigue can be observed; however, it is significantly below the threshold that could result in structural failure.

VI. CONCLUSION

This study presents a comprehensive approach for investigating the support of the draw gear under different loading conditions. A review of regulatory documents [4–7] was conducted, which define the main requirements for draw gear assemblies as well as the testing procedures.

In the course of the work, an extension of the methodology proposed in [13] and [14] was introduced. With the suggested modifications, the evaluation of components can also be performed within the plastic domain.

Computational models for the investigation of the draw gear support were developed, accurately reproducing the real behavior of the component under service conditions. These computational models can also be applied to the design sizing of other elements of the draw gear assembly.

Based on the developed models, a stress–strain analysis of the draw gear support was carried out, accounting for the occurrence of plastic deformations. Furthermore, a fatigue assessment was performed, establishing that the accumulated damage for all load cycles does not exceed D = 0.01.

The summarized results demonstrate that the draw gear support is capable of withstanding the required loads under all investigated load cases without risk of fatigue failure within the projected service life of 30 years.

For greater objectivity, it is necessary to verify the computational models by manufacturing a prototype of the investigated component and subjecting it to physical tests (both static and dynamic), in order to validate the results of the present work.

In addition, further research into crack propagation within the component could be conducted. Such investigations would provide valuable insight into the behavior of the product not only in the presence of defects arising from manufacturing processes, but also in cases where cracks are initiated during static testing.

ACKNOWLEDGMENT

The use of measuring equipment is supported by the Operational Program "Research, Innovation and Digitalization for Smart Transformation 2021 - 2027" under Project NoBG16RFPR002-1.014-0006-C01 "National center of excellence for mechatronics and clean technologies ".

REFERENCES

[1] M. Schüler, "Draw and Buffer Gear for A Railway Coupling, and Raiway Caupling". International Patent WA 2022/223394 A1, 27 October 2022.

[2] W. Simon, C. Colin and S. Maksym, "A review on design and testing methodologies of modern freight train draft gear system," *Railway Engineering Science,* pp. 127-151, 7 June 2021.[CrossRef]

[3] Y. Om Prakash and V. Nalinaksh S., "The influence of AAR coupler features on estimation of in-train forces," *Railway Engineering Science,* pp. 233-251, 18 February 2023. [CrossRef]

[4] Leafled UIC 520, Wagons, coaches and vans - Draw gear - Standardisation, 2003.

[5] Leaflets UIC 826, Technical provisions for the supply of screw couplings for tractive and trailing stock, UIC, 2004.

[6] EN-15566:2022 Railway applications - Railway Rolling stock - Draw gear and screw coupling, European Committee for Standardization, 2022.

[7] The European Commission, "Concerning the technical specification of interoperability relating to the subsystem 'rolling stock - freight wagons' of the trans - European conventional rail system," *Official Journal of the European Union,* 2006.

[8] A. Cernescu, I. Dumitru, N. Faur, N. Branzei and R. Bogdan, "The analysis of a damaged component from the connection system of the wagons," *Engineering Failure Analysis,* pp. 93-107, 05 December 2012.[CrossRef]

[9] M. Vuksic Popovic, J. Tanaskovic, D. Glisic, N. Radovic and F. Franklin, "Experimental and numerical research on the failure of railway vehicles coupling links," *Engineering Failure Analysis,* p. 105497, 21 May 2021.[CrossRef]

[10] F. Nový, M. Jambor, M. Petrů, L. Trško, S. Fintová and O. Bokůvka, "Investigation of the brittle fracture of the locomotive draw hook," *Engineering Failure Analysis,* pp. 305-312, 05 July 2019.[CrossRef]

[11] R. Ulewicz, F. Nový, P. Novák and P. Palček, "The investigation of the fatigue failure of passenger carriage drawhook," *Engineering Failure Analysis,* pp. 609-616, 21 June 2019.[CrossRef]

[12] M. V. Popović, J. Tanasković, Z. Starčević and N. Međedović, "Analysis of coupling system failures on freight trains," *ACTA TECHNICA JAURINENSIS,* vol. 16, no. 1, pp. 11-17, 2023.[CrossRef]

[13] S. Slavchev, Optimization of calculating process using numerical methods for calculation of the freight wagon body strength, Sofia: Technical university of Sofia, 2015.

[14] V. Maznichki, Simulation study of material fatigue in the railway bogie for freight, Sofia: Technical University of Sofia, 2021.

[15] Tiantian Wang, Zhikang Zhang, Zhiguo Li, Jingsong Xie, Weifeng Wang and Jingsong Yang, "Fatigue test and service performance evaluation of high-speed train hanging equipment bolts," *Structures,* p. 106202, 18 March 2024.[CrossRef]

[16] Zichun Zhou Honggang Lei, Bin Qiu, Shujia Zhang and Guoqing Wang, "Experimental Study on Fatigue Performance of M60 High-Strength Bolts with a Huge Diameter under Constant Amplitude Applied in Bolt–Sphere Joints of Grid Structures," *Applied sciences MDPI,* p. 8639, 29 August 2022. [CrossRef]

[17] W. Ramberg and W. R. 0sgood, "Description of stress-strain curves by three parameters Technical Note No. 902," NACA , Washington, 1943.[CrossRef]

[18] Eurocode 3: Design of steel structures - Part 1-9: Fatigue, EN 1993-1-9 : 2005, 2005.

[19] J. Bergström, C. Burman, J. Svensson, A. Jansson, C. Ivansson, Jing Zhou and S. Valizadeh, "Very High Cycle Fatigue of Two Ductile Iron Grades," *steel research international,* vol. 87, no. 5, pp. 614-621, 10 September 2015.[CrossRef]

[20] M. Benedetti, C. Santus, V. Fontanari, D. Lusuardi, F. Zanini and S. Carmignato, "Plain and notch fatigue strength of thick-walled ductile cast iron EN-GJS-600-3: A double-notch critical distance approach to defect sensitivity," *International Journal of Fatigue,* p. 106414, 10 July 2021. [CrossRef]

[21] S. Hübner, P. Trubitz, S. Henschel and L. Krüger, "Influence of Microstructure on Static and Cyclic Fracture Toughness of EN-GJS-600-3 Nodular Cast Iron," *International Journal of Metalcasting,* pp. 1217-1228, 08 August 2023. 1. [CrossRef]

[22] "Granta Materials Data for Simulation," Ansys, [Online]. Available: https://www.ansys.com/products/materials/materials-data-for-simulation. [Accessed 26 August 2025].